The M_w 7.9, 12 May 2008 Sichuan earthquake rupture measured by sub-pixel correlation of ALOS PALSAR amplitude images

Marcello de Michele[1], Daniel Raucoules[1], Cécile Lasserre[2], Erwan Pathier[2], Yann Klinger[3], Jérôme Van Der Woerd[4], Julia de Sigoyer[5], and Xiwei Xu[6]

[1]*French Geological Survey (BRGM), Land Use Planning and Natural Risks Division, Orléans, France*
[2]*Laboratoire de Géophysique Interne et Tectonophysique, CNRS, Université Joseph Fourier, Grenoble, France*
[3]*Institut de Physique du Globe de Paris, Laboratoire de Tectonique, Paris, France*
[4]*Institut de Physique du Globe, Strasbourg, France*
[5]*Ecole Normale Supérieure, Laboratoire de Géologie, Paris, France*
[6]*China Earthquake Administration, Institue of Geology, Beijing, China*

(Received October 9, 2008; Revised April 20, 2009; Accepted May 23, 2009; Online published January 26, 2011)

PALSAR L-band spaceborne Synthetic Aperture Radar (SAR) amplitude images are used to map the Sichuan earthquake rupture (China, M_w 7.9, 12 May 2008) and to identify the faults activated by the earthquake. A sub-pixel correlation method is used to retrieve the coseismic displacement field projected into the line of sight of the satellite and the horizontal along-track direction, and to map the surface rupture. The earthquake broke ∼270 km of the Beichuan fault and ∼70 km of the Guanxian fault, with a complex thrust-dextral slip mechanism. Along the southwestern part of the rupture, slip seems to be partitioned into a dextral-dominant component on the Beichuan fault and a thrust-dominant component on the Guanxian fault. Dextral slip may also be dominant at the northeastern tip of the Beichuan ruptured fault. Coseismic surface displacements reach on average 3 to 4 m in both measured directions. The SAR rupture mapping has proven complementary to field studies extending the zone of co-seismic displacements and identifying other possible co-seismic rupture strands.
Key words: Sichuan, earthquake, rupture, PALSAR, amplitude offsets.

1. Introduction

The Sichuan earthquake, M_w 7.9, struck the western Sichuan province on 12 May 2008. It represents one of the most disastrous earthquakes in Chinese history, severely affecting an area where little historical seismicity is reported (Gu *et al*., 1989; Chen *et al*., 1994) and a small convergence rate is measured (e.g., Gan *et al*., 2007). The hypocentre is located within the Longmen Shan at 19 km depth (USGS, 2008) between two major faults of the Longmen Shan thrust system, the Wenchuan and Beichuan faults (Fig. 1). The Longmen Shan thrust system bounds the eastern margin of the Tibetan plateau and is considered as a major thrust zone that was reactivated during the India-Asia collision (e.g., Tapponnier and Molnar, 1977; Avouac and Tapponnier, 1993; Chen and Wilson, 1996; Arne *et al*., 1997). However, contrasting geological evidence of sparse thrusting and marked dextral strike-slip faulting during the Quaternary (Burchfiel *et al*., 1995; Densmore *et al*., 2007) have led to models of dynamically sustained topography or crustal channel flow (Royden *et al*., 1997) limiting the role of earthquakes in mountain building and leaving the mechanism of long term strain distribution in this area as an open question. In this paper we use L-band spaceborne Synthetic Aperture Radar (SAR) from the PALSAR sensor onboard the ALOS satellite to map the Sichuan earthquake rupture and to identify the faults activated by the earthquake. By measuring the co-seismic offsets field in both the line of sight (i.e., slant range) and along track (i.e., azimuth) directions of the sensor, we gain an understanding of the rupture geometry, segmentation and sense of displacement. Our results complement field observations since parts of the ruptured areas are inaccessible impeding detailed field studies (Dong *et al*., 2008; Xu *et al*., 2009).

2. Data Analysis

A SAR system sends radar pulses to the ground and measures the amplitude and the phase of the backscattered signal. Each radar return is sampled at the base of an azimuth/slant range grid so that each echo corresponds to a geographic location, after geometric transformation. If between two radar acquisitions the position of a target changes we can precisely measure its corresponding offset by subpixel correlation analysis (e.g., Michel *et al*., 1999; Barbot *et al*., 2008). We use PALSAR amplitude images acquired before and after the Sichuan earthquake and measure the offset field generated by the earthquake in the range and azimuth directions by using the subpixel correlation routine implemented in the GAMMA software (Werner *et al*., 2005). We calculate offsets based on a 64 pixel window size on PALSAR fine beam single polarisation mode (FBS) data acquired during six parallel overlapping ascending tracks (Table 1).

Range offsets may suffer from limitations due to stereo-

doi:10.5047/eps.2009.05.002

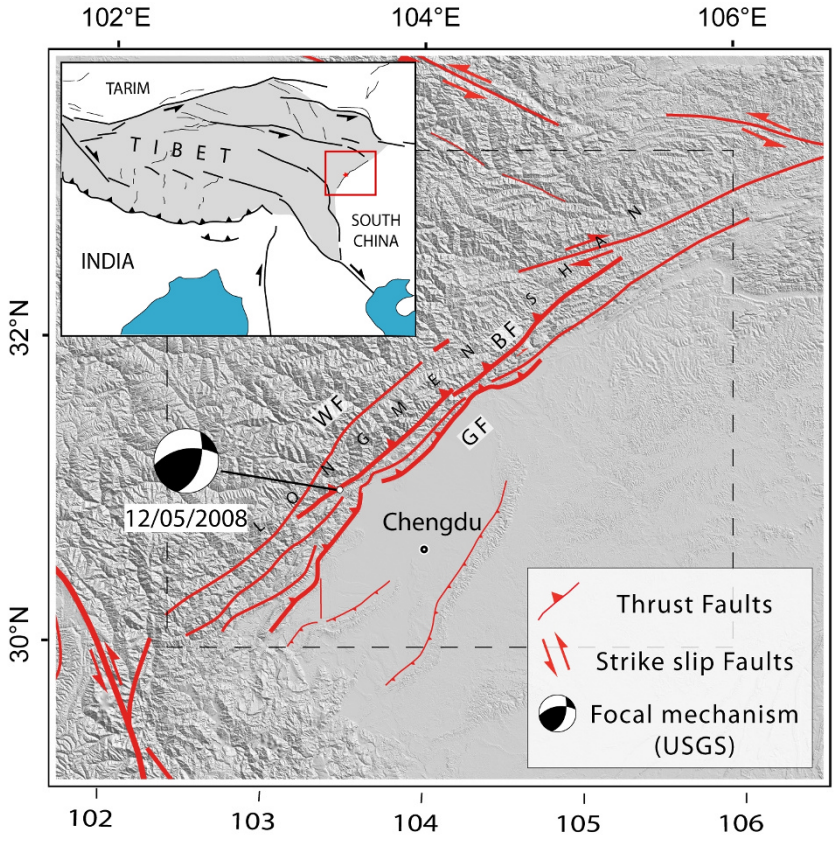

Fig. 1. The study area struck by the Sichuan earthquake. Quaternary active faults and their kinematics are plotted in red (modified from Tapponnier and Molnar, 1977). BF = Beichuan fault; WF = Wenchuan Fault; GF = Guanxian Fault. The dotted rectangle corresponds to the location of Figs. 2 and 3.

Table 1. PALSAR data used in this study.

Track	Date	Mode	Pixel size range/azimuth (m)
471	29/02/2008	Ascending	4.68/3.15
	31/05/2008		
472	31/01/2008	Ascending	4.68/3.15
	17/06/2008		
473	17/02/2008	Ascending	4.68/3.15
	19/05/2008		
474	05/04/2008	Ascending	4.68/3.15
	05/06/2008		
475	21/12/2007	Ascending	4.68/3.15
	22/06/2008		
476	08/04/2008	Ascending	4.68/3.15
	24/05/2008		

scopic effects. We reduce the stereoscopic contributions to coseismic range offset by adapting the methodology based on Principal Component Analysis presented in de Michele *et al.* (2008) to SAR amplitude images. We use the Digital Elevation Model (DEM) from the Shuttle Radar Topography Mission (SRTM) projected into radar geometry to estimate and reduce for the stereoscopic effect. Azimuth offsets may be affected by the influence of ionospheric electron density fluctuation occurring during the synthetic aperture (Gray *et al.*, 2000). For an L-band SAR, this phenomenon results in deca-km scale modulation in the position of optimum azimuth registration, which appears as oblique bands or 'azimuth streaks' in the offset image. Based on the observation that the azimuth streaks have a constant preferential orientation that does not coincide with the strike of the fault, we reduce this effect by an adaptive de-stripe filter originally developed by Leprince *et al.* (2007). It yielded a ∼56% average ionospheric correction on the azimuth offsets. The corrected offsets maps are then orthorectified and assembled (Figs. 2, 3).

3. Results

Figures 2 and 3 present maps of the range and azimuth offsets. We interpret steep offset gradients as the surface expressions of the earthquake rupture. The clearest offsets indicate that the rupture broke a 270 km-long major seg-

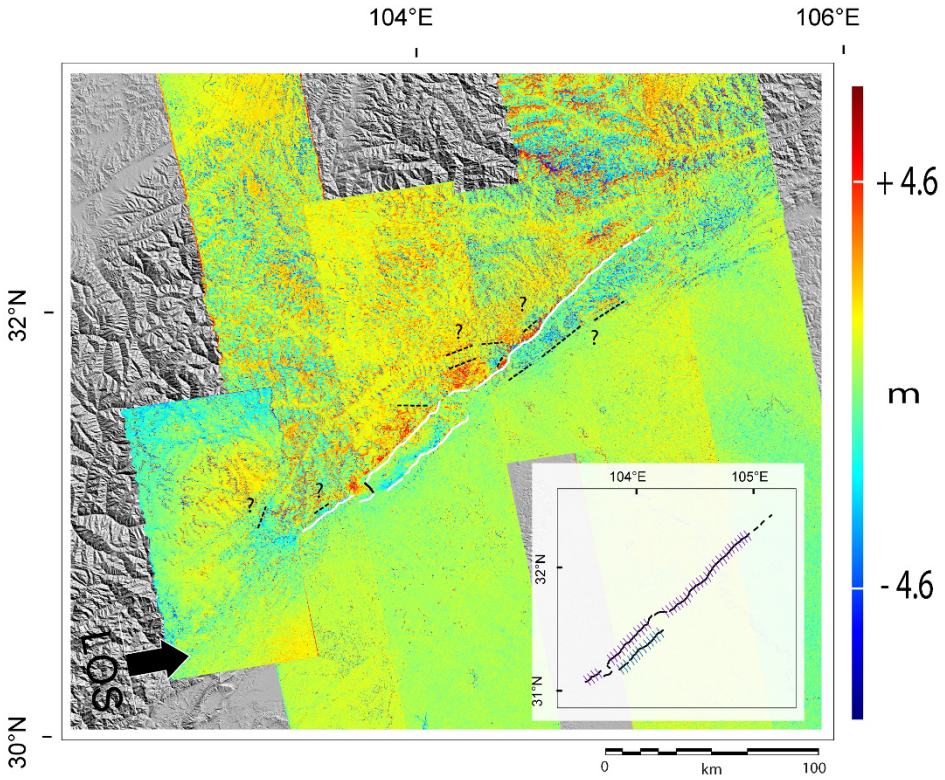

Fig. 2. Offsets in the range direction. Our interpretation of the rupture is plotted in white. Dark dashed lines represent possible rupture segments not yet observed in the field. The ~10 km rupture segment striking NW-SE (perpendicular to BF and GF ruptures) is presented in bold black (here and in Fig. 3). The inset represents the average location of profiles used in the stack to retrieve the offset plots in Fig. 4. See the inset of Fig. 3 for the satellite acquisition geometry.

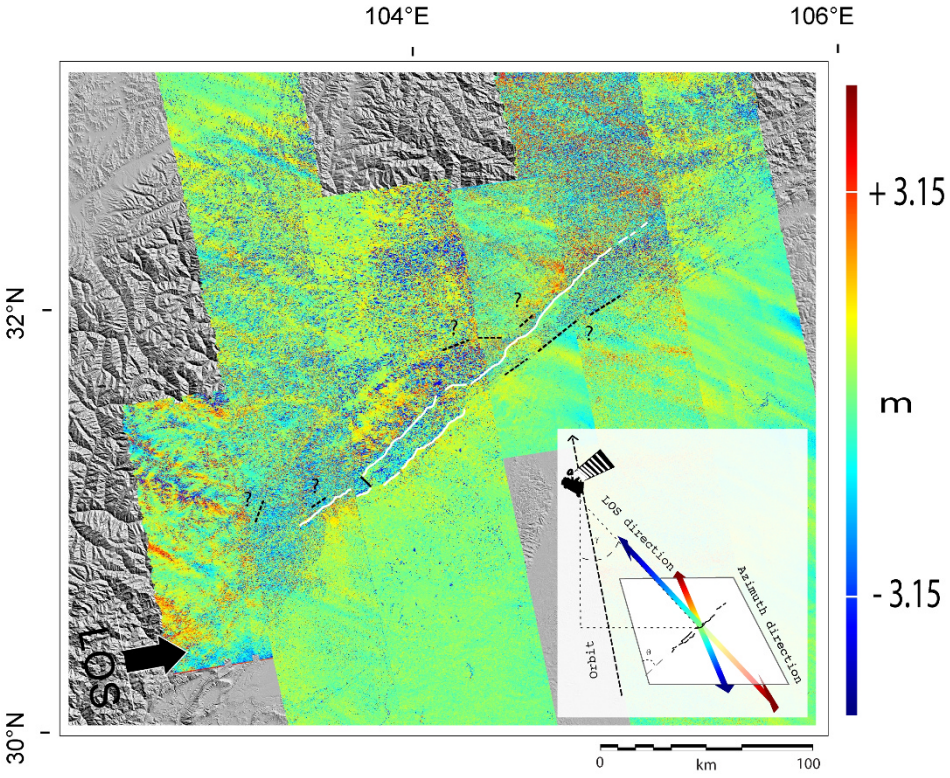

Fig. 3. Offsets in the azimuth direction (azimuth streaks reduced). Our interpretation of the rupture is plotted in white. Dark dashed lines represent possible rupture segments not yet observed in the field. The inset represents the PALSAR acquisition geometry relative to our case study. Colour scaled arrows indicate the slant range and azimuth direction of the measured offset relative to the rupture position. This is a key to interpret the sense of displacement in Figs. 2 and 3. γ = sight angle (34°), θ = angle between the rupture strike and azimuth direction (~65°).

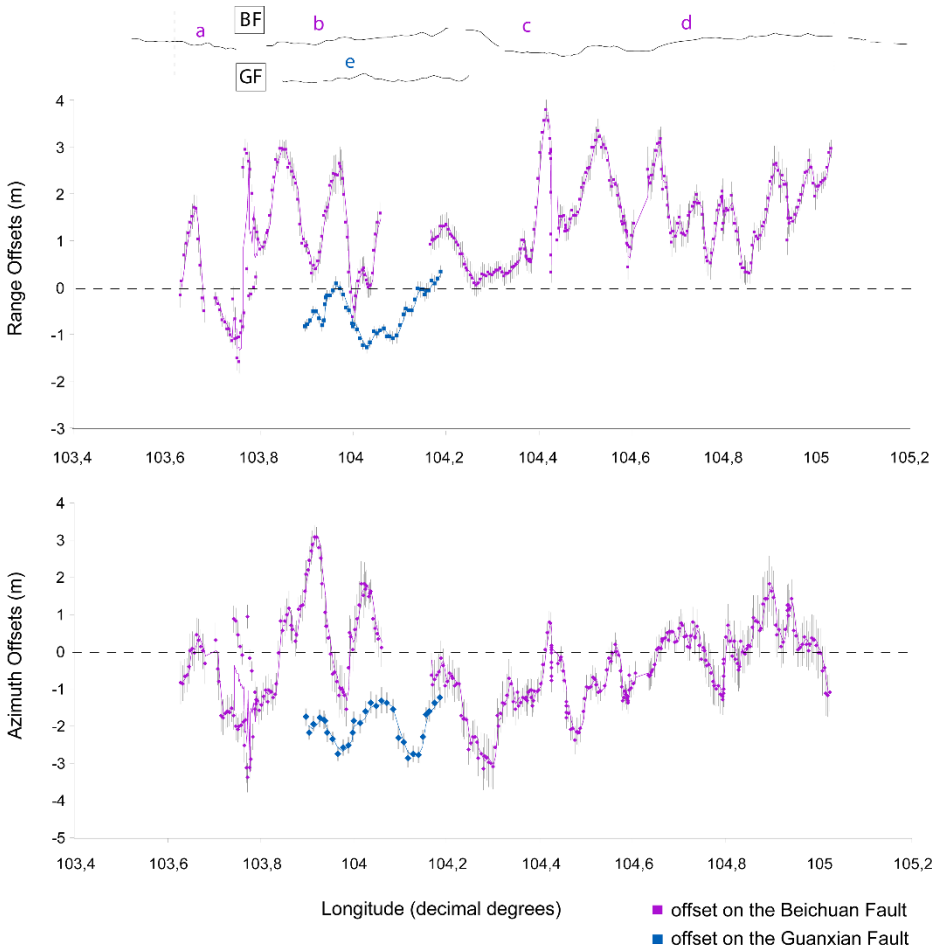

Fig. 4. Plot of range and azimuth offsets measured along the strike of the Beishuan fault (BF) and Guanxian Fault (GF) ruptures (plotted on top as reference). Major components of slip are dextral or reverse when offsets are positive and negative, respectively (see text for details). Longitude values are sampled along the strike of the rupture.

ment of the Beichuan Fault and a 70 km-long segment of the Guanxian Fault, both trending ∼N55E. It seems that another 10 km-long segment ruptured perpendicularly to the Beichuan and Guanxian Faults at the southwestern end of the Guanxian inferred rupture (grey segment in Fig. 2). Its signature is markedly visible on both offset maps. Our SAR rupture map is confirmed by field observations made by Dong *et al.* (2008) and Xu *et al.* (2009) and complements them in inaccessible areas. Further interpreting the SAR offset results, other ruptured fault segments might be evidenced although their signatures are less clear due to noise. These segments are typically inside the Longmen Shan, along the Wenchuan Fault and along the northeastern part of the Guanxian fault (black dotted lines in Figs. 2 and 3).

Figure 4 shows along-strike profiles of range and azimuth offsets across the Beichuan and Guanxian faults. Each measured point on the profiles in Fig. 4 results from the stack of 51 cross-strike profiles (according to the method proposed by Klinger *et al.* (2006) and Avouac *et al.* (2006) and implemented in Leprince *et al.* (2007)), providing an approximation of the offsets every 1 km. The plot in Fig. 4 yields an estimate of the magnitude and standard deviation of fault slips at the surface in range and azimuth directions. The standard deviation obtained during the stacking process provides an estimate of the precision of the offsets. This yields 0.31 m in azimuth and 0.24 m in range. The range offsets reach 3 and 2 m and the azimuth offsets reach 3.7 and 2.5 m on the Beichuan and Guanxian faults, respectively. However, our offset measurements are limited to two directions. Without a third component of the displacement and geometric constraints on the dip of the faults, we cannot make a quantitative comparison between horizontal and vertical slip values collected in the field and our offsets.

4. Discussion and Conclusions

Figures 2 and 3 display a complex rupture pattern that propagated on different fault segments. Results in Fig. 4 show the offset values in the range and azimuth direction. Taking into account the rupture strike, the satellite acquisition geometry (inset of Fig. 4) and field observations we can try to constrain the interpretation of the fault slip direction during the Sichuan earthquake based on range and azimuth offset values of Fig. 4. Assuming that the faults ruptured with a reverse dextral mechanism (Dong *et al.*, 2008; Xu *et al.*, 2009), we can state that positive offsets in both range and azimuth represent dextral-dominant slip while negative values in both directions correspond to thrust-dominant slip. With this in mind, we can infer the spatial partitioning of reverse and strike-slip faulting along the Beichuan

and Guanxian faults. We can argue that the Beichuan fault ruptured with a complex thrust-dextral mechanism while the Guanxian fault seems to have ruptured as an almost pure thrust. Dextral-reverse slip on segment *a* of the Beichuan fault becomes partitioned into a dextral dominant component on segment *b* of the Beichuan fault and thrust-dominant component on segment *e* of the Guanxian fault (Fig. 4). From segments *c* to *d* of the Beichuan fault, slip seems to evolve from dextral-reverse to dextral-dominant. This is not totally in agreement with field data, which show mostly thrust on the Guanxian fault, though equivalent reverse and dextral motion on the Beichuan fault.

In conclusion, sub pixel correlation of ALOS PALSAR amplitude images allowed us to map and measure the co-seismic rupture of the Sichuan earthquake. Our results complement field observations and thus allow a broader view of the rupture extension and segmentation.

Acknowledgments. The data used in this study were provided by the Japanese Space Agency (JAXA) through the CIEST agreement (Cellule d'Intervention et d'Expertise Scientifique et Technique) and the International Charter on Space and Major Disasters. M de Michele and D. Raucoules are funded by the research programs of BRGM.

References

Arne, D., B. Worley, C. Wilson, S. F. Chen, D. Foster, Z. L. Luo, S. G. Liu, and P. Dirks, Differential exhumation in response to episodic thrusting along the eastern margin of the Tibetan Plateau, *Tectonophysics*, **280**, 239–256, 1997.

Avouac, J. P. and P. Tapponnier, Kinematic model of active deformation in central Asia, *Geophys. Res. Lett.*, **20**, 895–898, 1993.

Avouac, J. P., F. Ayoub, S. Leprince, O. Konca, and D. V. Helmberger, The 2005, M_w 7.6 Kashmir earthquake: Sub-pixel correlation of ASTER images and seismic waveforms analysis, *Earth. Planet. Sci. Lett.*, **249**, 514–528, 2006.

Barbot, S., Y. Hamiel, and Y. Fialko, Space geodetic investigation of the coseismic and postseismic deformation due to the 2003 M_w7.2 Altai earthquake: Implications for the local lithospheric rheology, *J. Geophys. Res.*, **113**, B03403, doi:10.1029/2007JB005063, 2008.

Burchfiel, B. C., Z. Chen, Y. Liu, and L. H. Royden, Tectonics of the Longmen Shan and adjacent regions, *Int. Geol. Rev.*, **37**, 661–735, 1995.

Chen, S. F. and C. J. L. Wilson, Emplacement of the Longmen Shan Thrust-Nappe Belt along the eastern margin of the Tibetan Plateau, *J. Struct. Geol.*, **18**, 413–430, 1996.

Chen, S., C. J. L. Wilson, Q. Deng, X. Zhao, and Z. Luo, Active faulting and block movement associated with large earthquakes in the Min Shan and Longmen Mountains, northeastern Tibetan Plateau, *J. Geophys. Res.*, **99**, 24,025–24,038, 1994.

de Michele, M., D. Raucoules, H. Aochi, N. Baghdadi, and C. Carnec, Measuring coseismic deformation on the northern segment of the Bam-Baravat escarpment associated with the 2003 Bam (Iran) earthquake, by correlation of very-high-resolution satellite imagery, *Geophys. J. Int.*, **173**(2), 459–464, 2008.

Densmore, A. L., M. A. Ellis, Y. Li, R. Zhou, G. S. Hancock, and N. Richardson, Active tectonics of the Beichuan and Guanxian faults at the eastern margin of the Tibetan Plateau, *Tectonics*, **26**, TC4005, doi:10.1029/2006TC001987, 2007.

Dong, S., Y. Zhang, Z. Wu, N. Yang, Y. Ma, W. Shi, Z. Chen, C. Long, and M. An, Surface rupture and co-seismic displacement produced by the M_s 8.0 Wenchuan earthquake of May 12th, 2008, Sichuan, China: Eastward growth of the Qinghai-Tibet plateau, *Acta Geologica Sinica (English Version)*, **82**(5), 938–948, 2008.

Gan, W., P. Zhang, Z.-K. Shen, Z. Niu, M. Wang, Y. Wan, D. Zhou, and J. Cheng, Present-day crustal motion within the Tibetan Plateau inferred from GPS measurements, *J. Geophys. Res.*, **112**, B08416, doi:10.1029/2005JB004120, 2007.

Gray, A. L., K. E. Mattar, and G. Sofko, Influence of ionospheric electron density fluctuations on satellite radar interferometry, *Geophys. Res. Lett.*, **27**(10), 1451–1454, 2000.

Gu, G., T. Lin, and Z. Shi, *Catalogue of Chinese Earthquakes (1831 B.C.–1969 A.D.)*, Science Press, Beijing, China, 1989.

Klinger, Y., R. Michel, and G. C. P. King, Evidences for an earthquake barrier model from M_w 7.8 Kokoxili (Tibet) earthquake slip distribution, *Earth Planet. Sci. Lett.*, **242**, 354–364, 2006.

Leprince, S., S. Barbot, F. Ayoub, and J. P. Avouac, Automatic and precise orthorectification, coregistration, and subpixel correlation of satellite images, application to ground deformation measurements, *IEEE Trans. Geosci. Remote Sens.*, **45**, 1529–1558, 2007.

Michel, R., J. P. Avouac, and J. Taboury, Measuring ground displacements from SAR amplitude images: Application to the Landers earthquake, *Geophys. Res. Lett.*, **26**, 875–878, 1999.

Royden, L. H., B. C. Burchfiel, R. W. King, E. Wang, Z. Chen, F. Shen, and Y. Liu, Surface deformation and lower crustal flow in eastern Tibet, *Science*, **276**, 788–790, 1997.

Tapponnier, P. and P. Molnar, Active faulting and tectonics in China, *J. Geophys. Res.*, **82**(B20), 2905–2930, 1977.

USGS, http://earthquake.usgs.gov/eqcenter/recenteqsww/Quakes/us2008ryan.php, 2008.

Werner, C., U. Wegmuller, T. Strozzi, and A. Wiesmann, Precision estimation of local offsets between pairs of SAR SLCs and detected SAR images, *Proceedings of the Geoscience and Remote Sensing Symposium (IGARSS)*, 25–29 July 2005, IEEE International Volume 7, 4803–4805, 2005.

Xu, X., X. Wen, G. Yu, G. Chen, Y. Klinger, J. Hubbard, and J. Shaw, Co-seismic reverse- and oblique-slip surface faulting generated by the 2008 Mw 7.9 Wenchuan earthquake, China, *Geology*, **37**(6), 515–518, doi:10.1130/G25462A.1, 2009.

M. de Michele (e-mail: m.demichele@brgm.fr), D. Raucoules, C. Lasserre, E. Pathier, Y. Klinger, J. Van Der Woerd, J. de Sigoyer, and X. Xu